A predictive model to probe the impact of gravity and surface tension on rising wetting thin films

Zhen Luo and Shafigh Mehraeen*

Department of Chemical Engineering, University of Illinois at Chicago

810 South Clinton Street, Chicago, Illinois 60607, United States

E-mail: tranzabi@uic.edu

Phone: +1 (0)312 9968734. Fax: +1 (0)312 9960808

Abstract

Utilizing kinetic Monte Carlo simulations, we developed a three dimensional Ising lattice gas model to reveal the wetting mechanism of a liquid film rising along a vertical substrate. The model takes into account the impact of surface tension, gravity, interaction energy between liquid particles, and between liquid and substrate on the rise of the liquid film. We verify that in low gravitational acceleration regime, the growth of the liquid film follows the universal law of $\sqrt{t}$. As gravitational acceleration and surface tension vary, the simulation results show the detailed dynamics of the solid-liquid interface. Explicit analysis of the interface displacement and roughness under different gravitational accelerations and surface tensions is also presented.

Introduction

The spreading of liquid films on solid surfaces at nanometer scale plays a significant role in numerous technologies, including but not limited to painting, coating, micro-reactor and chemical sensors, which have received great attention over a century.[1–5] Recently, it was also shown that spreading liquids on solid surfaces can be applied to controllably position sub-10 nm particles into lithographically defined templates.[6–8] The development of these applications requires accurate knowledge of underlying dynamics of spreading, especially on surfaces with interfacial interactions occuring over a scale ranging from molecular distance to capillary length. At macroscopic scales, spreading of liquid films is precisely described by hydrodynamic theories that ignore the molecular structure of liquids.[9–13] At microscopic scale however, the origin of the universal laws that govern the spreading dynamics is not well understood.

The appearance of a spreading liquid film has been found to start from the formation of a molecularly thin liquid layer on the substrate.[14] This thin liquid layer spreads along the substrate faster than the rest of the liquid film. Using dynamic ellipsometry and x-ray reflectivity measurements,[15–23] it has been shown that on atomically smooth surfaces, one or few of these thin films advance faster than the macroscopic liquid film edge. Subsequently, this macroscopic liquid film spreads on top of such thin liquid layer, which may fuse into macroscopic extent at sufficiently long time. For nonvolatile liquids, it has been established that the linear extent of the thin layer grows proportional to $\sqrt{t}$, regardless of the nature of the species involved.[15] The law of $\sqrt{t}$ has been verified with different substrates and liquids in which the bottom thin liquid layer directly in contact with substrate spreads much faster.[16–18] Similar experiments performed for capillary rise geometries in which a thin liquid layer creeps upward on a solid wall, have also shown that the height of the liquid layer increases as $\sqrt{t}$ within certain time domain until the thin layer is broken by gravity.[19,20] As such, the universal law of $\sqrt{t}$ seems to be independent of the substrate, liquid, geometry as well as the size of the liquid molecules.

Computational approaches have been utilized to reveal the mechanism behind the rise of the thin liquid layer, and explain the time dependence of spreading. Several theoretical models have been proposed,[24–27] and molecular dynamics and Monte Carlo (MC) simulations have been performed.[15,28–33] In particular, Burlatsky *et al.* have proposed a microscopic 1D model,[15] which allows mass transport from reservoir to mono-molecularly thin layer, while its spreading is restricted by surface tension applied at the solid-liquid interface. The height of the thin layer was found via MC simulations to follow $\sim \sqrt{t}$. Using kinetic MC (KMC) simulations, Abraham *et al.* proposed a 3D lattice gas model predicting $\sqrt{t}$ time dependence of the rise.[26] Above mentioned models however, ignore the impact of gravity on the vertical spreading of the thin liquid layer.

In this paper, we present a 3D Ising lattice gas model to describe the rise of a thin liquid film against the gravity, and explain its fine structure. In our microscopic model, we account for the impact of gravity, surface tension, cohesive energy between liquid and substrate, and interaction energy between liquid particles on the rise of the liquid layer. Utilizing KMC simulations, we show that our model establishes the $\sqrt{t}$ behavior of rising liquid layer in the zero to low gravity regime, which is consistent with the original 2D Ising model in the absence of gravity studied before.[26] Additionally, we analyze the dynamics of spreading while varying gravitational acceleration, and surface tension. We report the impact of above mentioned parameters on the solid-liquid interface displacement, instantaneous interface velocity, and roughness.

Theory

Our lattice gas model mimics the experiment in which a substrate is partially immersed vertically into a liquid bath. Upon partial immersion, a macroscopic meniscus at the solid-liquid interface is created, followed by formation of a very thin liquid layer climbing up the vertical substrate against the gravity. We introduce a lattice model in which the dynamics of

the thin liquid layer is represented by motion of particles, which consist of liquid molecules, restricted to a 3D lattice. Every lattice site in this model can either be vacant or occupied by a liquid particle. In addition, the edge of the thin liquid layer, which represents the solid-liquid interface, is modeled by the dynamic boundary formed by the moving outermost particles.

We define a square lattice with unit lattice spacing $\Delta x = \Delta y = \Delta z = 1$ along x-, y-, and z-direction, respectively. We then specify the position of particles moving on the 3D square lattice by the position vector $\vec{r} = (x, y, z)$. Without loss of generality, we assume that z can only be 1 or 2, meaning that only two layers of particles parallel to the substrate are considered. Adding more layers will only slow our KMC simulations while it does not affect the dynamics of solid-liquid interface.

We define the dimensionless change in total energy for a given particles configuration in which a particle moves from site i to j by

$$\frac{\Delta E_{i\to j}}{kT} = \Delta G_{i\to j} + \Delta J_{i\to j} + \Delta A_{i\to j} + \Delta F_{i\to j}. \tag{1}$$

The first term in Eq. 1 denotes the work done by the gravity

$$\Delta G_{i\to j} = (y_j - y_i)g', \tag{2}$$

in which y_i and y_j are the y-coordinates of the site i and j, respectively, $g' = mg\Delta y/kT$ is the dimensionless gravitational acceleration, m is the particle mass, g is the dimensional gravitational acceleration, k is the Boltzmann constant, and T is temperature.

The second term in Eq. 1 is the contribution from particle-particle interaction denoted by

$$\Delta J_{i\to j} = (n_j - n_i)J, \tag{3}$$

where n_i and n_j are the total number of bonds with the nearest neighbors to be broken and made at site i and j, respectively, and J is the cohesion strength between neighbor particles,[25,26] nondimensionalized by kT.

The third term in Eq. 1 indicates the contribution from van der Waals interaction of liquid particles with the substrate characterized by the Hamaker constant $A > 0$,[25,34,35]

$$\Delta A_{i\to j} = A\left(\frac{1}{z_j} - \frac{1}{z_i}\right), \tag{4}$$

where z_i and z_j are the z-coordinates of site i and j, respectively, which can be either 1 or 2, corresponding to the bottom or top layer, respectively.

Interfacial energy at the solid-liquid interface is expressed by the last term in Eq. 1

$$\Delta F_{i\to j} = \sigma(y_j - y_i), \tag{5}$$

where $\sigma = \gamma\Delta x\Delta y/kT$ is the dimensionless surface tension, γ is the dimensional surface tension at the interface, and Δx and Δy is the lattice constant along the $x-$ and $y-$direction.[36]

Fig. 1A illustrates the 3D lattice model, where y is the axis perpendicular to the liquid bath (not shown). For clarity, we are not showing the underlying lattice grid. In Fig. 1A, red particles indicate the top layer of the liquid bath, blue and gray particles illustrate the top and bottom layers, and green particles depict the edge of the rising liquid layer where the surface tension is applied to particles vertical hops. Fig. 1B depicts the cross section of the rise of liquid layer, representing the four components of the energy change described in Eq. 1.

Numerical Simulations

Now, we parameterize the KMC simulations of the rise of the wetting liquid film, and describe the steps therein. Then, we present the statistical results for the impact of gravity and surface tension on the average interface displacement, instantaneous velocity, and

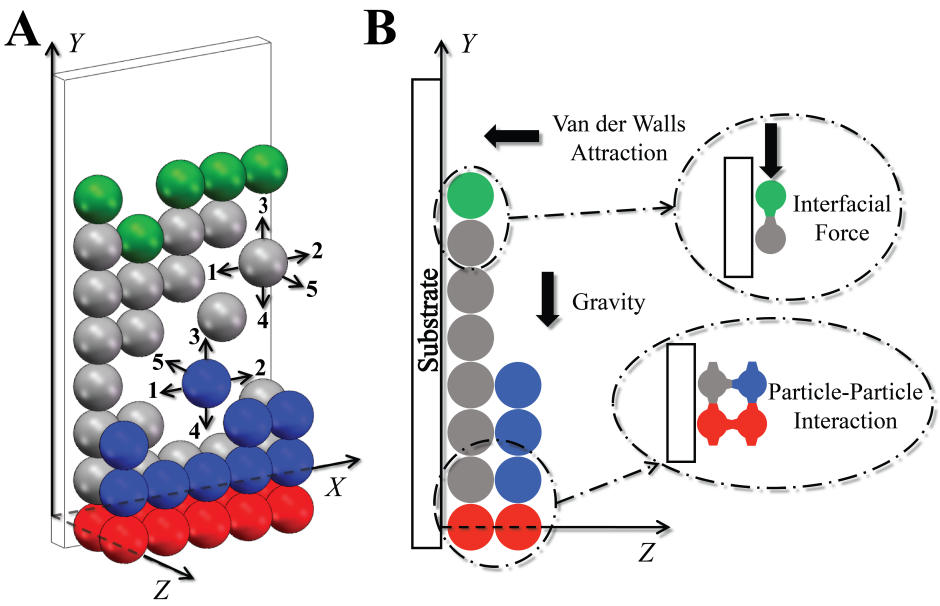

Figure 1. (A) The 3D schematics of the Ising lattice gas model, illustrating the rise of the liquid layer on the vertical substrate. Red particles represent the bulk liquid, gray and blue particles show the first and second layer of particles located at $z = 1$ and 2, respectively, and green particles illustrate the solid-liquid interface. Numbered arrows show four in-plane and one out-of-plane nearest neighbors.

(B) Cross section of the schematics, depicting the four component of the total energy, gravity, van der waals interaction with the substrate, nearest neighbor particle-particle interaction (bottom inset), and interfacial energy (top inset).

interface roughness of the liquid layer and its structure factor.

In our Ising lattice gas model, the mechanism of KMC simulations is to stochastically explore sequences of diffusive hops, by selecting events proportional to their transition rates.[37] According to the continuous time random walk,[38] the rate of transition is the particle-vacancy exchange rate from site i to site j defined by Kawasaki dynamics:[38]

$$r_{i\to j} = \nu \exp\left(-\frac{\Delta E_{i\to j}}{2kT}\right), \tag{6}$$

where $r_{i\to j}$ is the rate of a particle hopping from site i to j, and ν is the attempt frequency, which we set to the inverse of the number of destination sites. In our 3D model, for every hop, the number of destination sites is 5, *i.e.* As illustrated in Fig 1A, the gray particle at $z = 1$ has four in-plane and one out-of-plane direction whereas the blue particle at $z = 2$ has

four in-plane and one into-the-plane direction to move, all indicated by arrows. In general, the total possible destination sites is five, which is the same as number of nearest neighbors regardless of their occupation. According to Eq. 6, the rate of a given particle moving in a given direction certainly depends on the energy change for that move, or in essence, the details of local particles configuration.

We follow the definition of stochastic process in KMC method, and ensure the coordinate scale, maximum number of particles, and total KMC steps to be large enough to avoid finite-size effect. The steps in our KMC simulations are as follows:

1. As for the initial condition, we set the occupation number of all source sites (any x, $y = 1$, and $z = 1, 2$) to 1 (filled with particles). After a KMC hop at some later time, if any of these source sites becomes empty, we will fill it with a particle instantly. Thus, source sites are maintained as occupied at all times $t > 0$.

2. The rise of liquid layer takes place along y-direction. Therefore, we apply periodic boundary conditions along x-direction.

3. To achieve a high degree of non-volatility, we set the non-dimensionalized particle-particle interaction parameter, J, and van der Waal parameter, A, large enough to be in complete wetting regime.[39]

4. We calculate rates for all possible hops of particles using Eq. 6. Here, $\Delta E_{i\to j}$ is the energy change before and after a particular hop.

5. We select a move by randomly choosing a hop from the list of all possible hops proportional to the hopping rates.

6. We increment the KMC time by Δt (in KMC time unit), which is the time that has elapsed during one KMC step, given by:

$$\Delta t = -\frac{\ln(\rho)}{\sum_{\substack{i,j \\ i\neq j}} r_{i\to j}}, \tag{7}$$

where $0 < \rho \leq 1$ is a uniformly distributed random number.[40]

7. If a particle moves beyond $y = L_y$ (top side of the simulation box), its rates will be removed from the list of possible hops, not to be selected in the next selection cycle.

8. We update the new hopping rates, and repeat from step 5.

We define the simulation box size as $L_x = 100$ (*i.e.* $1 \leq x \leq 100$) unless otherwise mentioned, $L_y = 300$ (*i.e.* $1 \leq y \leq 300$), and $L_z = 2$ (*i.e.* $1 \leq z \leq 2$), and set the thermal energy to $kT = 1/3$ throughout all KMC simulations.

Results and discussion

With the setup above, we now look at the impact of gravity, g', and surface tension, σ, on the growth and interface roughness of the rising liquid layer.

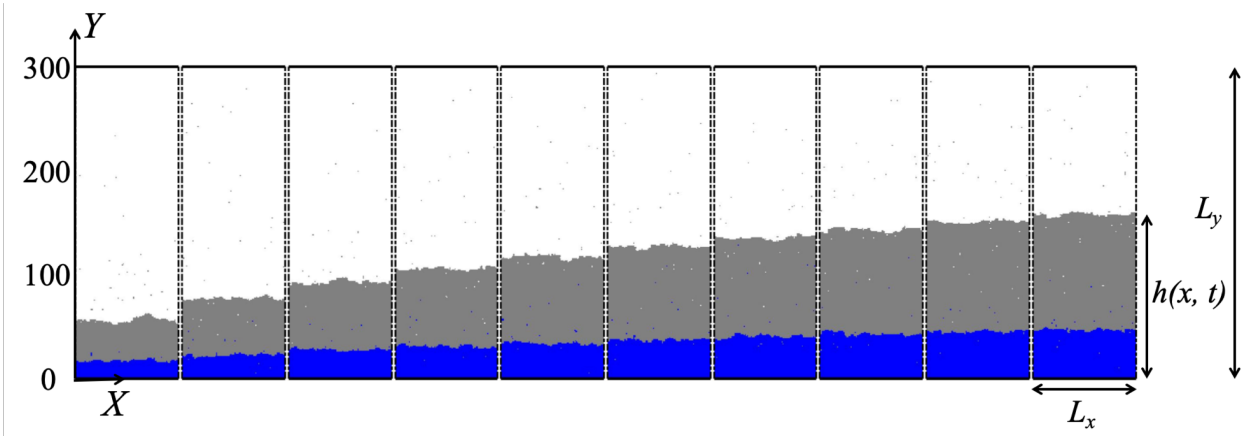

Figure 2. Top view of 10 snapshots, illustrating the rise of the liquid layer at different times, $t = 1 \times 10^7, \ldots, 10 \times 10^7$ with the interval of 10^7 in KMC time unit. Occupied sites at $z = 1$ and 2 are shown in gray and blue, corresponding to bottom and top layer, respectively. Empty sites are shown in white. Parameters used are $A = 30,\ J = 3,\ g' = 0,\ \sigma = 0$.

Fig. 2 illustrates KMC simulation results, from left to right, depicting 10 snapshots of the rise of the liquid layer along the vertical substrate in the absence of gravity and surface tension. As shown in Fig. 2, the first layer illustrated in gray, which is closer to the substrate, moves upward faster than the second layer, shown in blue. This is because as particles in

the first layer diffuse along the solid-liquid interface, vacancy defects are generated which diffuse downwards. Lowering van der Waals interaction, particles move from the 2nd layer ($z = 2$) to the 1st layer ($z = 1$) to fill the vacancy defects. As such the 1st layer advances faster than the 2nd layer. Once these vacancy defects reach to the bulk liquid at $y = 1$, they are immediately filled with new particles. Therefore, the rise of the bottom layer is due to the combined effects of vacancies advancing into the liquid bath, and the supplement from the 2nd layer of particles.

Our results in Fig. 2 also indicate that as particles diffuse and move up vertically, they create a connected path through their nearest neighbors from the top at solid-liquid interface to the bottom at the bulk liquid. We also observe free particles, without nearest neighbors, on the substrate above the solid-liquid interface, indicating the vapor phase. As these free particles diffuse, they either move downward and eventually get absorbed at the solid-liquid interface, or move upward and exit the simulation box in which case we remove the particles from the group of simulating particles. Defining the 1st layer of liquid by those particles connected through their nearest neighbors only, we now look at the average interface displacement of this 1st layer of particles and its progression in time.

To study the dynamics of average interface displacement of the rising liquid layer, we record the maximum local height of connected sites, $h(x, t)$, for $x = 1, 2, \ldots, L_x$ at all times, $t > 0$. Averaging over independent simulations, we find the average interface displacement, $\bar{s}(t)$, measured from initial configuration ($y = 1$), written as:

$$\bar{s}(t) = \frac{1}{L_x} \sum_{x=1}^{L_x} \langle h(x, t) \rangle - 1, \tag{8}$$

where $\langle ... \rangle$ stands for average over 200 independent KMC simulations for every x value while all other parameters (g', A, J, and σ) are unchanged.

In Fig. 3A, we present the results for the dynamics of the rising liquid layer for different gravitational acceleration constant, g'. In the absence of gravity (red curve, $g' = 0$), our results exhibit an initial ballistic dynamics, approximately varying linearly with time, *i.e.*

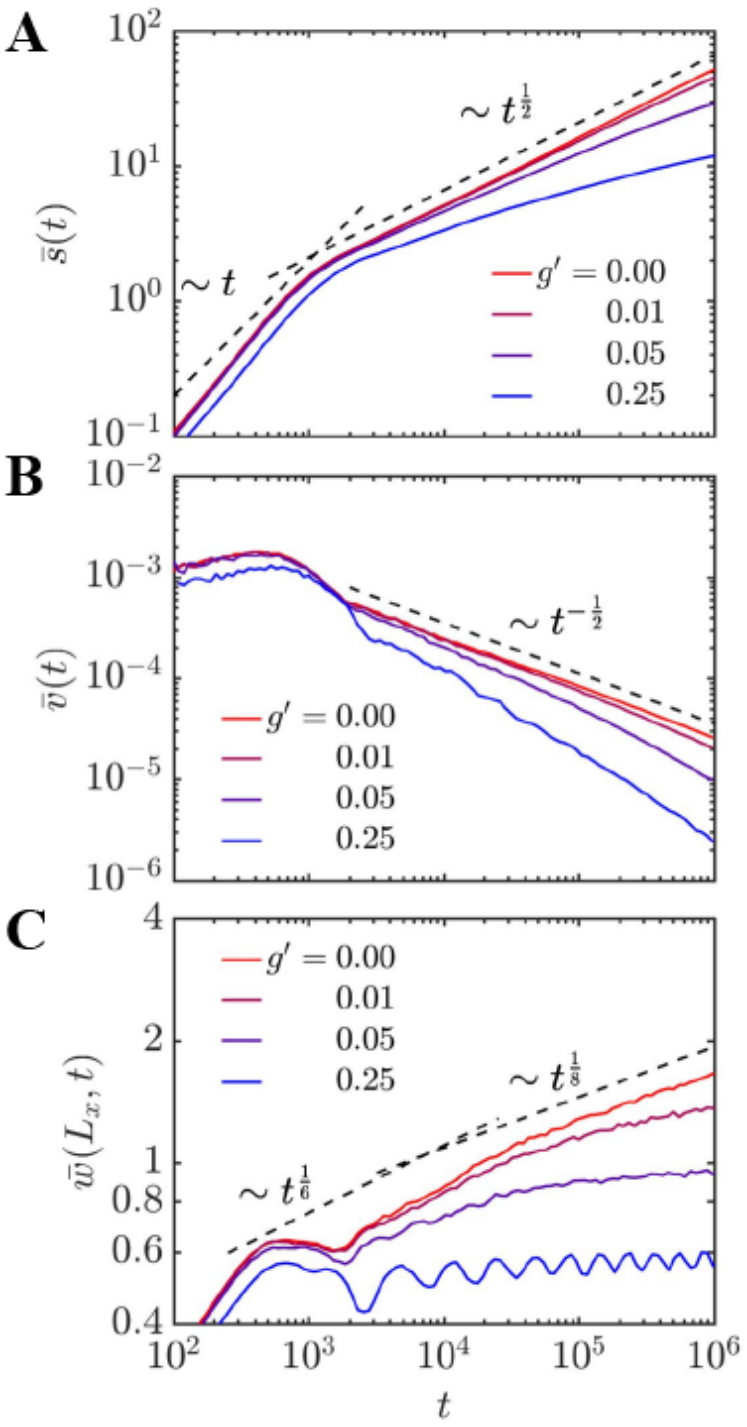

Figure 3. Log-log plot of evolution of the (A) average interface displacement, (B) instantaneous interface velocity, and (C) interface roughness of the rising liquid layer with time, t, in KMC time unit. Solid lines are averages over 200 independent KMC simulations with $A = 30$, $J = 3$, $\sigma = 0$, and $g' = 0$, 0.01, 0.05 and 0.25, from red to blue, respectively. Dashed lines are the guide for the eye.

$\bar{s}(t) \sim t$, followed by a diffusive dynamics, $\bar{s}(t) \sim \sqrt{t}$. We note that our results slightly deviate from true ballistic motion in which $\bar{s}(t)$ is exactly proportional to t. We attribute this deviation to the confinement along z-directions as we have considered only two layers at $z = 1$ and 2. Overall, this result is in agreement with the experimental results performed for capillary rise geometries.[19,20]

As gravitational acceleration, g', increases, the long time dynamics deviates from universal law of $\sqrt{t}$. The results suggest that gravity slows down the rate of upward wetting with average interface displacement $\bar{s}(t) \sim t^{\alpha}$, where $\alpha < 1/2$. Furthermore, we notice that gravity does not change the rate of wetting $(d\bar{s}(t)/dt)$ at shorter times while it reduces the rate at longer times. Although there is a small shift in $\bar{s}(t)$ at short time (blue curve in Fig. 3A compared to the red curve has shifted towards longer times), the rate of wetting has not changed at small time scales. This means that the rate of increase in average interface displacement is not affected by the gravity since the average interface displacement still advances linearly with time, *i.e.* $\bar{s}(t) \sim t$. One can also see this impact of gravity on the dynamics of wetting by looking at the instantaneous velocity of the edge of the liquid layer at $z = 1$.

The instantaneous velocity of the edge of the liquid layer (interface velocity) is subsequently calculated from time derivative of the average interface displacement, $\bar{s}(t)$:

$$\bar{v}(t) = \frac{d\bar{s}(t)}{dt}. \tag{9}$$

Fig. 3B, illustrates the interface velocity as time progresses for the same values of gravitational acceleration, g', shown in Fig. 3A. According to Fig. 3B, one can clearly see the deviation of interface velocity from universal law of $1/\sqrt{t}$ as the gravitational acceleration increases. We also notice that the interface velocity at small time scales ($t < 10^3$) slightly deviates from the constant $\bar{v}(t)$ for true ballistic motion. As discussed above, we attribute this deviation to the artificial confinement along z-direction applied to our Ising lattice gas model where particles can only hop between $z = 1$ and 2 planes.

The time dependent interface roughness is the standard deviation from average interface displacement, $\bar{s}(t)$, given by

$$\bar{w}(L_x, t) = \sqrt{\frac{1}{L_x} \sum_{x=1}^{L_x} \langle (h(x,t) - \bar{s}(t))^2 \rangle}. \tag{10}$$

Fig. 3C illustrates the evolution of interface roughness in time, calculated from Eq. 10 for the same values of gravitational acceleration shown in Fig. 3A and B. In the absence of gravity, our result in Fig. 3C is in clear qualitative agreement with the previous study conducted by Abraham *et al.*[26] As predicted by others,[26,41] in the absence of gravity, we also observe the cross over in $\bar{v}(t)$ from $t^{(1/6)}$ at intermediate times to $t^{(1/8)}$ at longer times shown by dashed lines in Fig. 3C. We also find that as gravitational acceleration, g', increases from 0 to 0.25, depicted from red to blue in Fig. 3C, respectively, the growth of interface roughness starts deviating from $t^{(1/6)}$ and $t^{(1/8)}$, at intermediate and longer times, respectively. In particular, when $g' = 0.25$ (blue curve in Fig. 3C), our result seems to suggest that there will be no overall growth in interface roughness.

The impact of gravity on the interface displacement, and roughness of the rising liquid layer can also be explained using the energy change of the MC hops in Eq. 1. According to this equation, gravity lowers the energy barrier for downward hops; hence, rates of downward hopping increase, leading to an overall directional diffusion downwards. Further increase in gravitational acceleration will completely hinder upward hopping, resulting to almost no growth in the interface displacement (not pictured). As for the interface roughness, gravity helps dampen fluctuations at the solid-liquid interface by lowering rates of upward hops, which will be energetically costly for large values of gravitational acceleration. In particular, for $g' = 0.25$ shown blue in Fig. 3C, interface roughness ceased to increase in time, leading to an overall constant value.

To better understand the extent of dimensionless gravitational acceleration, we compare different dimensionless and dimensional gravitational acceleration values. For this compari-

son, we assume the lattice spacing used in KMC simulations to be equal to the diameter of the simulating particles. This assumption is consistent with our particle representation in Fig. 1A. Furthermore, taking the particle diameter to be $\Delta x = \Delta y = \Delta z = 447$ nm, and the rising liquid to be water with density of 1000 kg/m^3, we find the particle mass to be 4.68×10^{-17}kg. We also nondimensionalize the energy by $kT = 4.11 \times 10^{-21}$J. Using the relation for dimensional gravitational acceleration in Eq. 2, we present the mapping between dimensionless and dimensional gravitational acceleration, g' and g, respectively, in Table 1. It is noteworthy that g can be tuned experimentally using a centrifugal adhesion balance (CAB) equipment developed by Tadmor *et al.*[42–45]

In CAB, a centrifugal arm holds the substrate at one end while rotating perpendicular to the gravitational field. With a setup in which the substrate is hanging from a hinge like a pendulum, and $0 \leq \alpha \leq 180^o$ being the counter clockwise angle between the vertical line going through the hinge (axis of rotation) and substrate, the gravitational acceleration along the substate will be $R\omega^2 \sin(\alpha) + g\cos(\alpha)$. Here, ω is the angular velocity, and R is average distance of the liquid film from the axis of rotation. With this definition of R, we are assuming variation of R along the liquid film is negligible. Obviously, depending on α being smaller or larger than 90 degrees, one would increase or decrease g with ω, respectively. With this setup, the force perpendicular to the substate, which is $R\omega^2 \cos(\alpha) - g\sin(\alpha)$, is mapped on to the Hamaker constant A in Eq. 4. These are the steps we envision for experimental verification of the KMC simulations. However, additional work is still warranted to perform above experiment and verify the simulation results shown in Fig. 3, which is left for a future research.

Table 1. The mapping between dimensionless and dimensional gravitational acceleration

g'	g (m/s^2)
0	0
0.01	1.97
0.05	9.83
0.25	49.2

Now, we turn into the impact of surface tension, in the absence of gravity ($g' = 0$), on the dynamics of the rising liquid layer. In rising liquid layer, dynamics of solid-liquid interface is directly impacted by the surface tension as formulated in Eq. 1 and 5. According to this dynamics, the surface tension only affects the particles at solid-liquid interface. Essentially, interfacial tension tends to minimize the length of solid-liquid interface; therefore, interfacial perturbations with large wave lengths become energetically costly to form. In KMC simulations, surface tension will penalize the total energy change associated with hops that create perturbation in positive $y-$direction; thus, making upward movement energetically unfavorable. This leads to lowering the likelihood of selecting interface particles tending to move along positive $y-$direction, rendering a delay in the rise of the liquid layer. We observe this delay (a shift in time) in the progression of interface displacement by increasing dimensionless surface tension parameter, σ, from 0 to 3.2, corresponding to red to blue curves in Fig. 4A, respectively.

Results in Fig. 4A suggest that the surface tension does not alter dynamics of the liquid layer as it still exhibits an initial rise slightly larger than t, followed by a diffusive dynamics with interface displacement proportional to $\sqrt{t}$. We speculate that this small deviation of interface displacement from linearly varying at short time might be due to the confinement considered along the z-direction in our 3D model. Nonetheless, these results from our 3D Ising lattice gas model are in qualitative agreement with the previous work reporting the growth of liquid film height using a one dimensional Ising model.[15]

Interface velocity profile of the rising liquid layer is shown in Fig. 4B for the same range of surface tension depicted in Fig. 4A. The small deviation in interface displacement from ballistic move at short time exhibits small deviation in the interface velocity illustrated in Fig. 4B as well. According to Fig. 4B, we estimate this deviation in the interface velocity to be in the order of $\sim 10^{-3}$. Our results also suggests that increasing surface tension, shown from red to blue in Fig. 4B, lowers the interface velocity at short time. This impact is more pronounced compared to that at long time as the shifts of interface velocity in time is larger

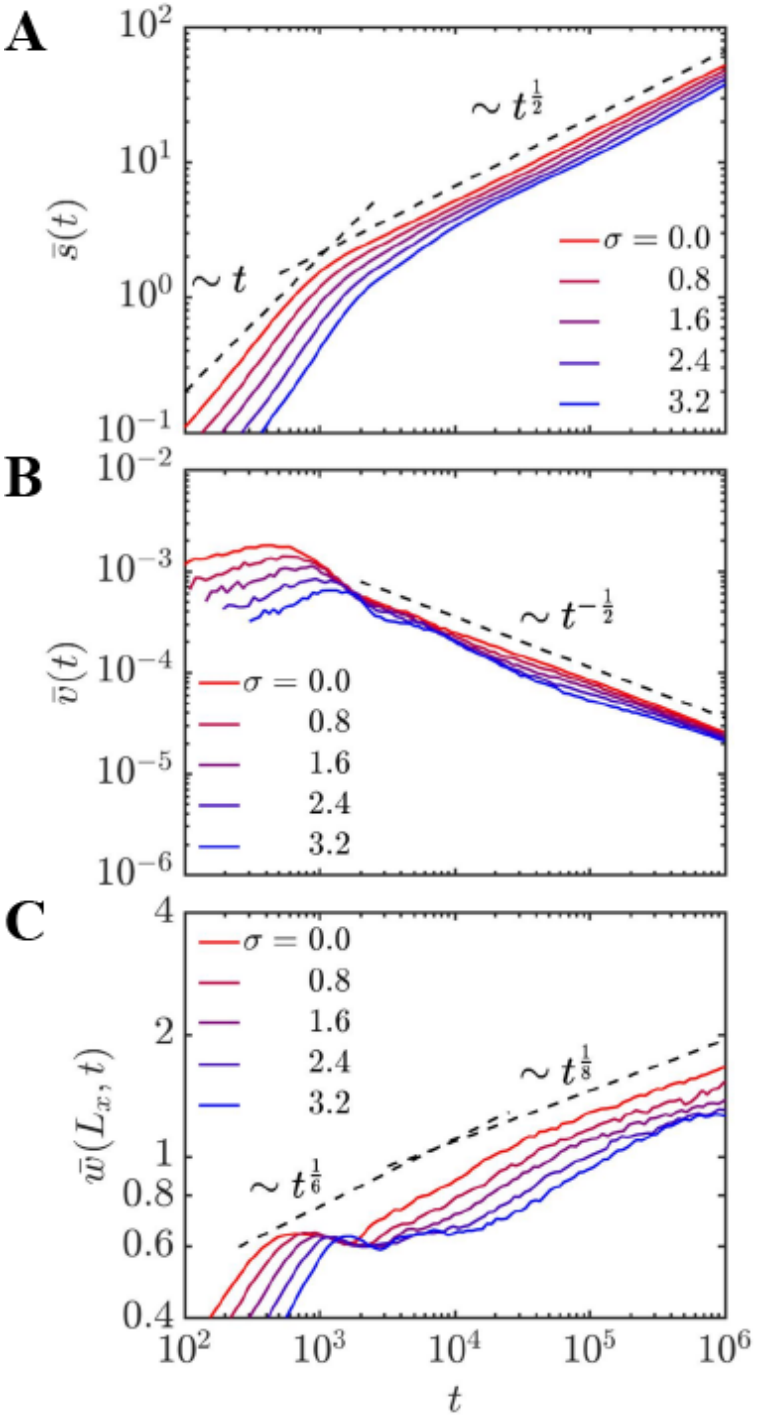

Figure 4. Log-log plot of growth of the (A) average interface displacement, (B) instantaneous interface velocity, and (C) interface roughness of the rising liquid layer with time, t, in KMC time unit. Solid lines are averages over 200 independent simulations with $A = 30$, $J = 3$, $g' = 0$, $\sigma = 0$, 0.8, 1.6, 2.4, and 3.2, from red to blue, respectively. Dashed lines are the guide for the eye.

at short time.

Interface roughness, $\bar{w}(L_x, t)$, is also affected by the surface tension in that as surface tension increases, evolution of perturbation at the interface is retarded, leading to a delay in growth of interface roughness. This delay is manifested by a shift toward larger time, as illustrated in Fig. 4C with σ being the same as those in Fig. 4A and B, increasing from red to blue, respectively. In particular, we observe the kinetic roughening of the interface [26,41] in the transition from $t^{(1/6)}$ at intermediate times to $t^{(1/8)}$ at long times, as σ increases. However, to verify whether or not interface roughness grows with $t^{(1/8)}$ at long time for large values of σ, KMC simulations need to be run for at least an order of magnitude longer than 10^6 KMC time unit performed in this work. We leave this verification to a future work.

Table 2 represents the mapping between dimensionless and dimensional surface tension used in Fig. 4. For this mapping, we utilize above-mentioned lattice spacing and thermal energy (kT) and invoke the surface tension definition in Eq. 5. We are hypothesizing that by using different liquids and substrate materials one could potentially tune the surface tension. We notice that the dimensional values for surface tension in Table 2 is rather small. To work with these dimensionless values for surface tension yet model larger dimensional surface tension, one would need to consider smaller lattice spacing. However, surface tension only slows the rise by affecting the interfacial particles upward hops. Therefore, increasing γ and consequently σ will only cause KMC simulations to spend a lot of time on moving bulk particles as opposed to interfacial particles, manifesting a shift along the time axis in the interface displacement, velocity, and roughness, as shown in Fig. 4C.

Table 2. The mapping between dimensionless and dimensional surface tension

σ	γ (mN/m)
0	0
0.8	1.65×10^{-5}
1.6	3.29×10^{-5}
3.2	6.58×10^{-5}

It is important to note that the interface roughness is also affected by the size of the

simulation box, L_x, which is an upper bound for the size of the largest wave length that can be presented by our KMC simulations. To gain more information on the impact of the size of the simulation box (largest wave length) on the interface roughness, we look at the variation of structure factor of interface roughness with size of simulation box in the presence of gravity and surface tension. The structure factor of interface roughness is calculated from

$$S(k,t) = \langle \xi_k(t)\xi_{-k}(t) \rangle \tag{11}$$

where $\langle ... \rangle$ stands for average over 200 independent KMC simulations, and $\xi_k(t)$ is the Fourier transform of the difference of interface displacement from the average, *i.e.*

$$\xi(x,t) = h(x,t) - \bar{s}(t). \tag{12}$$

The Fourier transform is written as

$$\xi_k(t) = \sum_{j=1}^{n} \xi(x_j,t) e^{-2\pi(j-1)(k-1)/n}, \quad k = 1, ..., n \tag{13}$$

in which $x_j = j\Delta x = j$, and $n = L_x/\Delta x = L_x$. In the absence of gravity and surface tension, the Fourier transform of interface roughness is expected to behave

$$S(k,t) \sim k^{-(2\alpha+1)} \tag{14}$$

at long times, where α is the roughness exponent.[26,41] It can be shown that α is linked to the order of correlation of interface roughness with the largest wave length via

$$\bar{w}(L_x,t) \sim L_x^{\alpha} \tag{15}$$

at long times.[26,41] We verified this behavior in $S(k,t)$ measured at 5 logarithmically spaced KMC times between $t = 10^3$ and 10^6 with $L_x = 512$ averaged over 200 independent KMC simulations, as shown in Fig. 5A, indicating $\alpha \approx 0.50$, which is in reasonable agreement with

the previous report.[26]

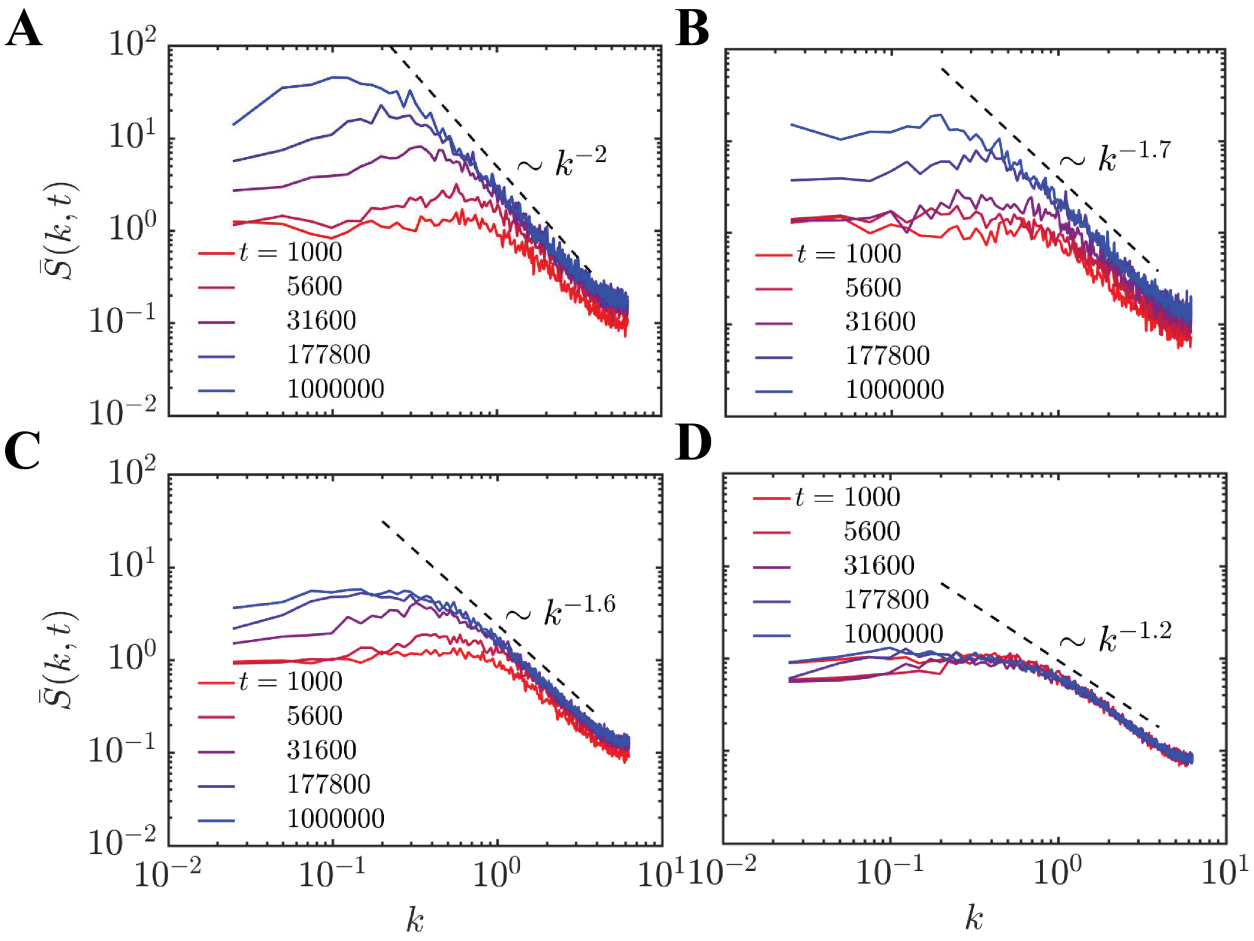

Figure 5. Structure factor of the interface roughness at 5 logarithmically spaced KMC time unit between $t = 10^3$, and 10^6, from red to blue, respectively, averaged over 200 independent KMC simulations for (A) $g' = \sigma = 0$, (B) $g' = 0, \sigma = 3.2$, (C) $g' = 0.05, \sigma = 0$ and (D) $g' = 0.25, \sigma = 0$. Other parameters are $A = 30, J = 3, L_x = 512,$ and $L_y = 300$. Dashed lines are the guide for the eye, illustrating k^{-2}, $k^{-1.7}$, $k^{-1.6}$ and $k^{-1.2}$ behavior in panels A, B, C and D respectively.

Our results suggest that in the absence of gravity, as dimensionless surface tension increases from $\sigma = 0$ to 3.2, roughness exponent decreases from $\alpha = 0.5$ to 0.35, as shown in Fig. 5B. We rationalize the dependence of interface roughness on the largest wave length as follows. Surface tension tends to flatten the interface, making large wave lengths energetically prohibitive to form. Formation of such long wave modes require concerted motion of points along the interface, rendering a rise in the interfacial energy. As such, impact of surface tension on the dampening of the largest wave mode becomes more pronounced.

According to Eq. 15, increasing the surface tension lowers interface roughness, and hence α. Similarity of Fig. 5A and B reveals that the underlying dynamics of rising liquid layer is only retarded once surface tension is applied at the interface. Hence, in the presence of surface tension, dynamics similar to that in the absence of surface tension will be observed yet at some longer time.

Likewise, in the absence of surface tension, we found that gravity has similar impact on the interface roughness. Fig. 5C and D illustrates the decay of structure factor as time increases in the presence of gravity, $g' = 0.05$ and 0.25, rendering the roughness exponent $\alpha \approx 0.35$ and 0.1 (see Supporting Information for $g' = 0.01$). Small α implies that interface roughness is nearly independent of the longest interfacial wave mode that can be formed theoretically during the rise of liquid layer, which indicates that interface roughness correlation in Eq. 15 may no longer hold. The fact that structure factor for large enough gravitational acceleration at different KMC times almost overlap, as illustrated in Fig. 5D, is also indicative of interface roughness being nearly independent of time as well as the longest wave mode, justifying the possible break down of interface roughness correlation mentioned above. Furthermore, smaller value of α extracted from Fig. 5C and D compared to that from Fig. 5B, suggests that the impact of gravity on dampening interface roughness is more evident than that of surface tension. We conjecture that is because gravitational force is a distributed force field, applied to every point in the bulk fluid; consequently, affecting every upward hop in KMC simulation. However, surface tension is a force applied to every point along the interface. Thus, concentrating only on the interface displacement, and so less effective.

Conclusions

We developed a 3D Ising lattice gas model to understand the impact of surface tension and gravity on the dynamics of a very thin liquid layer rising along a flat substrate. Utilizing our 3D lattice gas model in KMC simulations, we have shown that in the presence of surface

tension alone, interface vertical displacement follows the $\sqrt{t}$ universal law; however, the dynamics of liquid motion is retarded, leading to a delay in transition from ballistic to diffusive motion (t to $\sqrt{t}$) in interface displacement. We have demonstrated that in the presence of gravity, interface displacement deviates from $\sqrt{t}$ universal law to the extent that at large value of gravitational acceleration, the interface will cease to rise. While in the presence of surface tension, spatiotemporal fluctuations of interface roughness can be dynamically rescaled at long times, we found that in the presence of large gravitational acceleration, these fluctuations cannot dynamically be rescaled.

Overall, our work has allowed us to address how surface tension and gravity affect the interfacial dynamics. Here, we only considered single component fluid. However, additional work is warranted to show the interface as well as flow dynamics during rising (wetting) and falling (dewetting) of complex liquid films where nanoparticles are suspended. Understanding this dynamics will help unravel mechanisms of directed self-assembly of nanoparticles during dewetting of such complex liquid films.

Acknowledgement

Z. Luo and S. Mehraeen gratefully acknowledge seed funding from the College of Engineering at University of Illinois, Chicago.

Supporting Information Available

This material is available free of charge via the Internet at `http://pubs.acs.org/`.

References

(1) De Gennes, P. G. Wetting: statics and dynamics. *Reviews of Modern Physics* **1985**, *57*, 827–863.

(2) Forcada, M. L.; Mate, C. M. Molecular layering during evaporation of ultrathin liquid films. *Nature* **1993**, *363*, 527–529.

(3) Leger, L.; Joanny, J. F. Liquid spreading. *Reports on Progress in Physics* **1992**, *55*, 431–486.

(4) Cazabat, A. M. How does a droplet spread. *Contemporary Physics* **1987**, *28*, 347–364.

(5) Voue, M.; De Coninck, J. Spreading and wetting at the microscopic scale: recent developments and perspectives. *Acta Materialia* **2000**, *48*, 4405–4417.

(6) Asbahi, M.; Mehraeen, S.; Wang, F.; Yakovlev, N.; Chong, K. S. L.; Cao, J.; Tan, M. C.; Yang, J. K. W. Large area directed self-assembly of sub-10 nm particles with single particle positioning resolution. *Nano Letters* **2015**, *15*, 6066–6070.

(7) Asbahi, M.; Mehraeen, S.; Lim, K. T. P.; Wang, F.; Cao, J.; Tan, M. C.; Yang, J. K. W. Template-induced structure transition in sub-10 nm self-assembling nanoparticles. *Nano Letters* **2014**, *14*, 2642–2646.

(8) Mehraeen, S.; Asbahi, M.; Fuke, W.; Yang, J. K. W.; Cao, J.; Tan, M. C. Directed self-assembly of sub-10 nm particles: role of driving forces and template geometry in packing and ordering. *Langmuir* **2015**, *31*, 8548–8557.

(9) Tanner, L. H. Spreading of silicone oil drops on horizontal surfaces. *Journal of Physics D: Applied Physics* **1979**, *12*, 1473.

(10) Joanny, J. F.; De Gennes, P. G. Upward creep of a wetting fluid: a scaling analysis. *Journal De Physique* **1986**, *47*, 121–127.

(11) Brochard, F. Spreading of liquid drops on thin cylinders: The manchon-droplet transition. *The Journal of Chemical Physics* **1986**, *84*, 4664–4672.

(12) Brochard-Wyart, F.; De Gennes, P. G.; Hervet, H. Wetting of Stratified Solids. *Advances in Colloid and Interface Science* **1991**, *34*, 561–582.

(13) Ausserre, D.; Picard, A. M.; Leger, L. Existence and role of the precursor film in the spreading of polymer liquids. *Physical Review Letters* **1986**, *57*, 2671–2674.

(14) Hardy, W. B. The spreading of fluids on glass. *The London, Edinburgh, and Dublin Philosophical Magazine and Journal of Science* **1919**, *38*, 49–55.

(15) Burlatsky, S. F.; Oshanin, G.; Cazabat, A. M.; Moreau, M.; Reinhardt, W. P. Spreading of a thin wetting film: Microscopic approach. *Physical Review E* **1996**, *54*, 3832–3845.

(16) Heslot, F.; Cazabat, A. M.; Levinson, P.; Fraysse, N. Experiments on wetting on the scale of nanometers: Influence of the surface energy. *Physical Review Letters* **1990**, *65*, 599–602.

(17) Tiberg, F.; Cazabat, A. M. Self-assembly and spreading of nonionic trisiloxane surfactants. *Europhysics Letters* **1994**, *25*, 205–210.

(18) Cazabat, A. M.; De Coninck, J.; Hoorelbeke, S.; Valignat, M. P.; Villette, S. Influence of substrate heterogeneities on the spreading of a drop. *Physical Review E* **1994**, *49*, 4149–4153.

(19) Heslot, F.; Cazabat, A. M.; Fraysse, N. Diffusion-controlled wetting films. *Journal of Physics: Condensed Matter* **1989**, *1*, 5793–5798.

(20) Cazabat, A. M.; Fraysse, N.; Heslot, F. Thin wetting films. *Colloids and Surfaces* **1991**, *52*, 1–8.

(21) Daillant, J.; Benattar, J. J.; Leger, L. Ultrathin films in wetting evidenced by x-ray reflectivity. *Physical Review A* **1990**, *41*, 1963–1977.

(22) Albrecht, U.; Otto, A.; Leiderer, P. 2-dimensional liquid polymer diffusion: experiment and simulation. *Physical Review Letters* **1992**, *68*, 3192–3195.

(23) Perez, E.; Schaffer, E.; Steiner, U. Spreading dynamics of polydimethylsiloxane drops: Crossover from Laplace to van der Waals spreading. *Journal of Colloid and Interface Science* **2001**, *234*, 178–193.

(24) Abraham, D. B.; Collet, P.; De Coninck, J.; Dunlop, F. Langevin Dynamics of Spreading and Wetting. *Physical Review Letters* **1990**, *65*, 195–198.

(25) Lukkarinen, A.; Kaski, K.; Abraham, D. B. Mechanisms of fluid spreading: Ising model simulations. *Physical Review E* **1995**, *51*, 2199–2202.

(26) Abraham, D. B.; Cuerno, R.; Moro, E. Microscopic model for thin film spreading. *Physical Review Letters* **2002**, *88*, 206101.

(27) Oshanin, G.; De Coninck, J.; Cazabat, A. M.; Moreau, M. Microscopic model for spreading of a two-dimensional monolayer. *Journal of Molecular Liquids* **1998**, *76*, 195–219.

(28) Nieminen, J. A.; Alanissila, T. Spreading dynamics of polymer microdroplets: A molecular-dynamics study. *Physical Review E* **1994**, *49*, 4228–4236.

(29) Haataja, M.; Nieminen, J. A.; Alanissila, T. Dynamics of the spreading of chainlike molecules with asymmetric surface interactions. *Physical Review E* **1996**, *53*, 5111–5122.

(30) De Coninck, J. Spreading of chain-like liquid droplets on solids. *Colloids and Surfaces A: Physicochemical and Engineering Aspects* **1996**, *114*, 155–160.

(31) Bekink, S.; Karaborni, S.; Verbist, G.; Esselink, K. Simulating the spreading of a drop in the terraced wetting regime. *Physical Review Letters* **1996**, *76*, 3766–3769.

(32) Heine, D. R.; Grest, G. S.; Webb, E. B. Spreading dynamics of polymer nanodroplets. *Physical Review E* **2003**, *68*, 061603.

(33) Popescu, M. N.; Dietrich, S. Model for spreading of liquid monolayers. *Physical Review E* **2004**, *69*, 061602.

(34) Abraham, D. B.; Heinio, J.; Kaski, K. Computer simulation studies of fluid spreading. *Journal of Physics A: Mathematical and General* **1991**, *24*, L309–L315.

(35) Heinio, J.; Kaski, K.; Abraham, D. B. Dynamics of a microscopic droplet on a solid surface: Theory and simulation. *Physical Review B* **1992**, *45*, 4409–4416.

(36) Young, T. An essay on the cohesion of fluids. *Philosophical Transactions of the Royal Society of London* **1805**, *95*, 65–87.

(37) Battaile, C. C. The kinetic Monte Carlo method: Foundation, implementation, and application. *Computer Methods in Applied Mechanics and Engineering* **2008**, *197*, 3386–3398.

(38) Newman, M. E. J.; Barkema, G. T. *Monte Carlo Methods in Statistical Physics*; Oxford University Press, 1999.

(39) Domb, C. *Phase transitions and critical phenomena*; Academic Press, 2000.

(40) Binder, K.; Heermann, D.; Roelofs, L.; Mallinckrodt, A. J.; McKay, S. Monte Carlo simulation in statistical physics. *Computers in Physics* **1993**, *7*, 156–157.

(41) Barabasi, A. L.; Stanley, H. E. *Fractal concepts in surface growth*; Cambridge University Press, 1995.

(42) Tadmor, R.; Das, R.; Gulec, S.; Liu, J.; N'guessan, H. E.; Shah, M.; Wasnik, P. S.; Yadav, S. B. Solid-liquid work of adhesion. *Langmuir* **2017**, *33*, 3594–3600.

(43) Tadmor, R.; Bahadur, P.; Leh, A.; N'guessan, H. E.; Jaini, R.; Dang, L. Measurement of Lateral Adhesion Forces at the Interface between a Liquid Drop and a Substrate. *Physical Review Letters* **2009**, *103*, 266101.

(44) N'guessan, H. E.; Leh, A.; Cox, P.; Bahadur, P.; Tadmor, R.; Patra, P.; Vajtai, R.; Ajayan, P. M.; Wasnik, P. Water tribology on graphene. *Nature Communications* **2012**, *3*, 1242.

(45) Leh, A.; N'guessan, H. E.; Fan, J.; Bahadur, P.; Tadmor, R.; Zhao, Y. On the Role of the Three-Phase Contact Line in Surface Deformation. *Langmuir* **2012**, *28*, 5795–5801.

Graphical TOC Entry